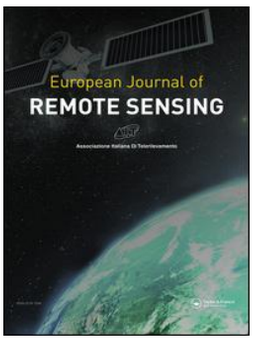

European Journal of Remote Sensing

ISSN: (Print) 2279-7254 (Online) Journal homepage: http://www.tandfonline.com/loi/tejr20

Terrestrial Remote Sensing techniques to complement conventional geomechanical surveys for the assessment of landslide hazard: The San Leo case study (Italy)

Margherita Cecilia Spreafico, Luigi Perotti, Federico Cervi, Marco Bacenetti, Gabriele Bitelli, Valentina Alena Girelli, Emanuele Mandanici, Maria Alessandra Tini & Lisa Borgatti

To cite this article: Margherita Cecilia Spreafico, Luigi Perotti, Federico Cervi, Marco Bacenetti, Gabriele Bitelli, Valentina Alena Girelli, Emanuele Mandanici, Maria Alessandra Tini & Lisa Borgatti (2015) Terrestrial Remote Sensing techniques to complement conventional geomechanical surveys for the assessment of landslide hazard: The San Leo case study (Italy), European Journal of Remote Sensing, 48:1, 639-660, DOI: 10.5721/EuJRS20154835

To link to this article: https://doi.org/10.5721/EuJRS20154835

Published online: 17 Feb 2017.

European Journal of Remote Sensing - 2015, 48: 639-660
doi: 10.5721/EuJRS20154835
Received 03/12/2014, accepted 28/06/2015

European Journal of Remote Sensing
An official journal of the Italian Society of Remote Sensing

www.aitjournal.com

Terrestrial Remote Sensing techniques to complement conventional geomechanical surveys for the assessment of landslide hazard: The San Leo case study (Italy)

Margherita Cecilia Spreafico[1], Luigi Perotti[2]*, Federico Cervi[1], Marco Bacenetti[2], Gabriele Bitelli[1], Valentina Alena Girelli[1], Emanuele Mandanici[1], Maria Alessandra Tini[1] and Lisa Borgatti[1]

[1]DICAM, Alma mater Studiorum University of Bologna, Viale Risorgimento 2, 40136, Bologna
[2]Earth Sciences Department, University of Torino, Via Valperga Caluso 35, 10125, Torino
*Corresponding Author, e-mail address: luigi.perotti@unito.it

Abstract

The San Leo village, located near to Rimini (northern Italy), was built in the medieval period on the top of a calcarenite and sandstone plateau, affected by lateral spreading associated with secondary rock falls and topples. In fact, a number of landslides endangered the historical town since centuries. In order to describe the structural features driving these slope instability phenomena, a complete Terrestrial Laser Scanner (TLS) survey all around the San Leo cliff was performed. Moreover, Close-Range Photogrammetric (CRP) surveys and conventional geomechanical surveys on scanlines have been carried out. The 3D geometry of the cliffs was extracted and critical areas have been investigated in detail using dense Digital Surface Models (DSMs) obtained from CRP or TLS. The results were used to define the structural features of the plateau, to recognize more fractured areas, and to perform kinematic analyses, in order to assess the joint sets predisposing to slope instability at the cliff scale. The creation of a 3D model was also fundamental for the implementation of the geological model to be used in numerical modelling for hydrogeological characterization and slope stability analyses.

Keywords: Terrestrial Laser Scanner, Close-Range Photogrammetry, geomechanical survey, landslides, San Leo, Italy.

Introduction

In the northern Apennines, historical towns were often built on the top of isolated rock plateaux, for defense purposes. The typical geological setting of these slabs, with a brittle rock unit lying on a ductile substratum, can promote slope instability phenomena, known as lateral spreading. Their evolution can pose a severe risk to the towns themselves and to their notable cultural heritage. Several Authors investigated similar rock spreading phenomena, indicating among the main influencing factors the deformability contrast between the involved units [Casagli, 1994], the overburden weight of the rock slab [Pasuto

and Soldati, 2013] and the erosion of the softer material [Bozzano et al., 2008]. As stated by Pasuto and Soldati [2013] for similar contexts, the presence of a well-developed system of joints can be considered as a controlling factor for the evolution of the phenomena. Besides the structural setting of the slab, a further predisposing factor is the groundwater flow developing inside the rock mass. The presence of perennial and ephemeral springs at the base of the cliffs can lead to accelerated erosion processes causing, together with minor landslides, the progressive undermining of the rock slab [Borgatti et al., 2015; Spreafico et al., 2015a; Spreafico et al., 2015b]. Even in this case, the discontinuity network plays a primary role, allowing the groundwater flow inside the slab and driving its direction and velocity. Therefore, the structural characterization of the rock mass is fundamental in the frame of landslide hazard assessment procedure.

Usually, the analyses of the geological structures are performed by geomechanical field surveys. These can be challenging, due to the difficulty to access steep, high and dangerous rock faces or due to the large dimensions of the area to be surveyed. Terrestrial remote sensing techniques, including both Terrestrial Laser Scanning (TLS) and Close-Range Photogrammetry (CRP), represent a useful complement to conventional field mapping and rock mass discontinuity characterization [Coggan et al., 2007; Ferrero et al., 2009; Bistacchi et al., 2011; De Souza et al., 2013]. Both these techniques were proven to be useful in the study of rock slopes by several Authors [Bitelli et al., 2004; Abellan et al., 2006; Oppikofer et al., 2009; Sturzenegger et al., 2009a; Jaboyedoff et al., 2010; Nguyen et al., 2011; Giardino et al., 2011; Matasci et al., 2012; Humair et al., 2013; Wolter et al., 2013; Barbarella and Fiani, 2013; Di Salvo and Lo Brutto, 2014]. The comprehension of the main strengths and limitations of the survey techniques (i.e., geomechanical survey, TLS and CRP) permits to understand how they can be complemented to achieve a better characterization of the rock mass. This can be done analyzing the workflow and comparing the results. For example Assali et al. [2014] compared data sets obtained in a limestone quarry in the French Alps, assessing the higher accuracy of TLS and photogrammetry, while Sturzenegger et al. [2009b] provide recommendations for optimizing the use of these techniques.

In order to assess the effectiveness of these survey techniques, the San Leo rock slab was chosen as a case study (Fig. 1). The particular interest of this case study comes from a number of different reasons: i) the distinctive geological and geomorphological settings; ii) the possibility to build the full model in three dimensions of a complex geological object with subvertical and overhanging cliffs; iii) the landslide risk condition affecting valuable cultural heritage assets.

Data extracted through fracture mapping techniques were used to perform kinematic analyses, in order to investigate the possible failure mechanisms in critical areas. Furthermore, the results of the analyses permitted to recognize the most fractured areas and to relate these zones with the main structural lineaments. This allowed the initial hypotheses about the structural features of the plateau to be strengthened. The results of the presented work lay the groundwork for understanding the mechanisms promoting the slope instability in the plateau, providing the data for further and more advanced slope stability analyses.

Geological context and typical slope instability phenomena

The San Leo rock slab is formed by rocky Epiligurian geological units, named the San Marino limestone and the Monte Fumaiolo sandstone units (Fig. 1). The rock mass lies on Ligurian Argille Varicolori scaly clays [CARG project, 2013].

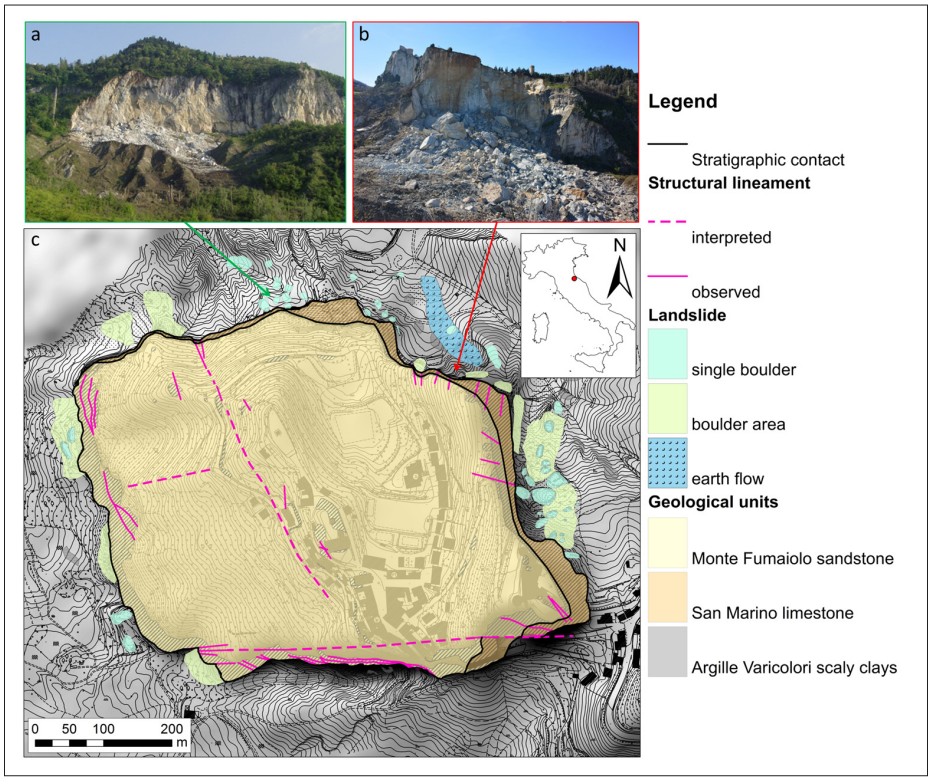

Figure 1 - Views of the (a) 2006 (b) 2014 landslides. (c) Geological/Structural map of the area (2007).

The San Leo slab is about 500 m wide and 600 m long and has a general north-westward dipping with an angle of about 10°. The subvertical and overhanging cliffs, up to 100 m high, which border the slab, are the product of subsequent rock falls and topples [Benedetti et al., 2013]. The slab is severely tectonized and crossed by a number of joint sets and faults. The overall slope deformation can be described as a rock spreading with associated rock falls and topples, partly developing along pre-existing discontinuities. Moreover, the underlying scaly clays and loose deposits are involved in earth slides and flows, which progressively undermine the foot of the slab. Rock falls and topples, occurring along the perimeter of the slab may involve volumes of rock variable from a few m^3 to several thousand of m^3. In particular, detachments of rock blocks along pre-existing discontinuities occurred frequently in the cliff underneath the castle and at the entrance of the town. One recent example is the landslide occurred the night between the 29th and the 30th of November 2008, when a small-scale rock fall (volume equal to about 6 m^3) affected the cliff overlooking the only access road to the town, blocking the transit for several days. Major slope instability events involved the collapse of large portions of rocks mass, often in areas undermined by the removal of the underlying clay-rich terrains. These kind of phenomena are typical in the northern cliffs, e.g. the 2006 and 2014 landslides (Fig. 1). In particular, in 2006 the detachment of 50,000 m^3 of material caused the reactivation of an earth flow-earth

slide [Benedetti et al., 2013]. At the end of February 2014, another large event occurred in the north-eastern side of the slab, with an estimated volume of approximately 300,000 m^3 [Spreafico et al., 2014]. It caused a retrogression of the cliff of 30 m, threatening some private and public buildings located on the top of the slab near to the scarp and again reactivating an earth flow-earth slide.
In these major events, the presence of subvertical discontinuities, joined with the undermining of the cliff, was proven to control the onset of slope instability and the volume of the failure [Spreafico et al., 2015b]. In general, for both minor and major events, the discontinuity network assumes a key role in the evolution of slope instability phenomena at different spatial and temporal scales, controlling both the groundwater infiltration and flow inside the slab and the kinematics of slope failure.

Data collection

The extraction of object geometries from laser scans and photogrammetric images has been a topic of research for several years. Both techniques offer the opportunity to collect reliable and dense 3D point data over objects or surfaces. In particular, soon after the laser scanner devices had been developed to a commercial level, it was speculated that photogrammetry would be totally replaced by laser scanners. On the other hand, it was asserted that image matching techniques would be able to produce the same point clouds of LiDAR instruments without using expensive devices. However, it has afterwards become more clear that the methods are complementary and can be deployed also according to the project and site specifics [Nex and Rinaudo, 2011].
In this work, based on these issues and with the aim of defining the 3D geometry of the slab and to characterize the discontinuity network, all the cliffs were surveyed using a TLS. CRP and conventional geomechanical surveys have been carried out in selected areas of the cliff in order to compare the geo-structural features extraction capabilities of the three different techniques (Fig. 2).

Conventional geomechanical surveys

Conventional geomechanical surveys were carried out along scanlines, according to the methods suggested by the International Society for Rock Mechanics [ISRM, 1978]. In particular, the position, orientation, spacing, aperture and frequency of the fracture planes or traces intersecting the scanline were reported. Moreover, the infilling material was examined and some basic parameters, as the rock wall strength (Joint Compression Strength JCS) and roughness profiles (Joint Roughness Coefficient JRC) were measured, to derive the strength properties of the discontinuities [Barton and Choubey, 1977]. A summary of the possible sampling bias, i.e. censoring, truncation, length and f-bias, with proposed corrections is reported in Zhang and Einstein [1998, 2000]. This permitted to infer some of the mechanical properties, e.g. cohesion and friction angle, and hydraulic properties related to the discontinuities characteristics, e.g. the equivalent hydraulic conductivity of the rock mass.
Surveys were conducted in different parts of the plateau, and two of them were considered for comparison and validation of remote sensing techniques. The first of these surveys took place on the northern side of the slab, in the scarp of the 2006 landslide, while the second surveyed area is located on the southern cliff, below the unique access road to the town of San Leo (Fig. 3).

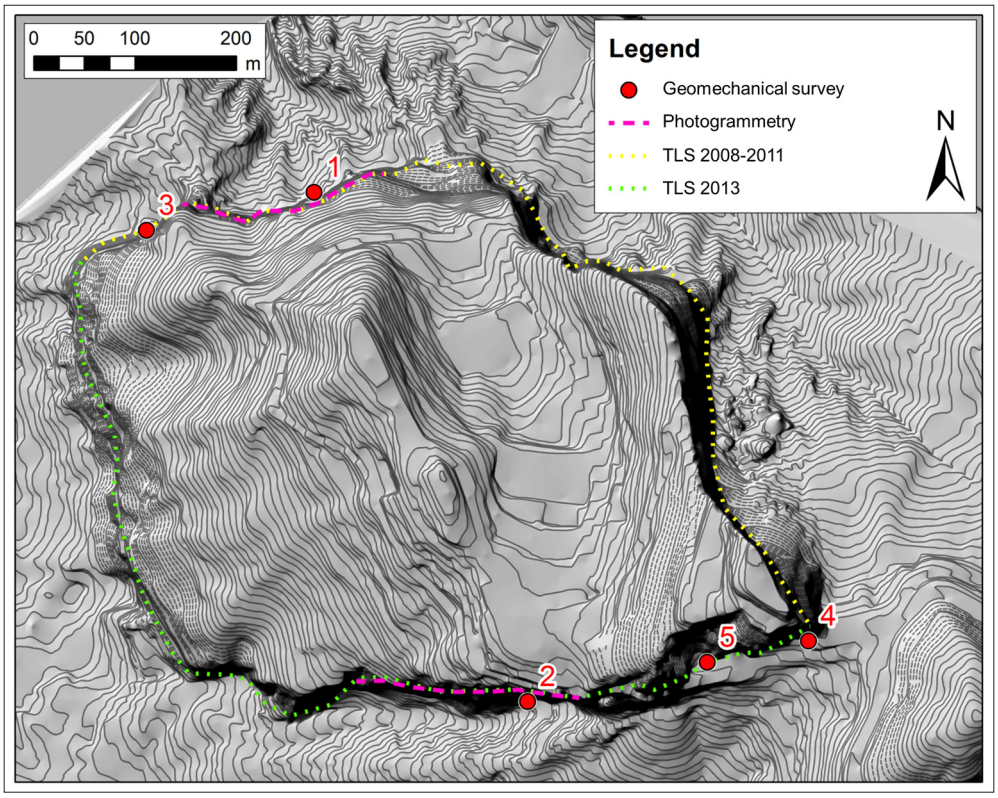

Figure 2 - Localization of the TLS, CRP and geomechanical surveys.

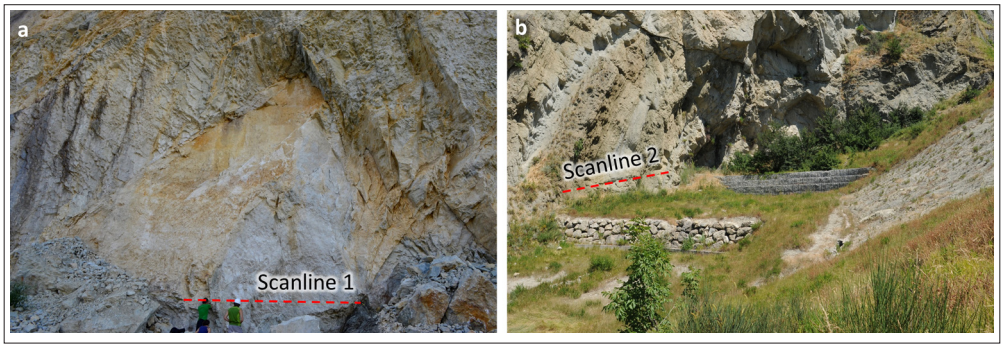

Figure 3 - Areas surveyed along scanlines, a) scanline 1 on the northern cliff and b) scanline 2 on the southern cliff. See Figure 2 for location

Terrestrial Laser Scanner (TLS)

TLS surveys were undertaken using a Riegl VZ-400 system coupled with a calibrated digital camera. Due to the topography of the area, to the lack of intervisibility between survey positions and to the difficulties to access to certain areas, a careful planning of the

survey was essential. A series of scans of north and east San Leo cliffs were already taken in 2008 and 2011 with a Riegl Z420i laser scanning system. The survey all around the rock slab was completed in 2013, scanning the south and west cliff from 16 positions around the slab, with a sampling step of about 20 mm on the rock surface (Fig. 4). Due to the topography of the area to be surveyed, it was not always possible to perform a close-range survey, therefore the long-range mode of the system was also used.
Images were also collected during the surveys with a high resolution calibrated digital camera, obtaining an average Ground Sample Distance (GSD) of 2-3 cm, in the areas described by high density cloud (point spacing about 2 cm). These images were used to colour the point clouds, obtaining over 900 million points with associated RGB value (Fig. 4a). Point cloud alignment and georeferencing were performed using natural and artificial targets (spheres or retro-reflective target tape) surveyed through a three dimensional network measured by integrated topographical and GNSS techniques, to obtain the absolute ETRF2000 (2008.0 epoch) position of total station standpoints. In the global georeferencing process, a GNSS station, located below the castle, was used as master station to frame the TLS survey to a global reference system. Its coordinates were derived using the permanent GNSS stations of Firenze, San Marino, Perugia and Medicina. The 3D geocentric positions were finally projected in the cartographic system UTM-WGS84 (zone 33); the ellipsoidal heights were converted in the orthometric ones by means of a model provided by Emilia-Romagna Region. An overall accuracy of 2-3 cm may be estimated.

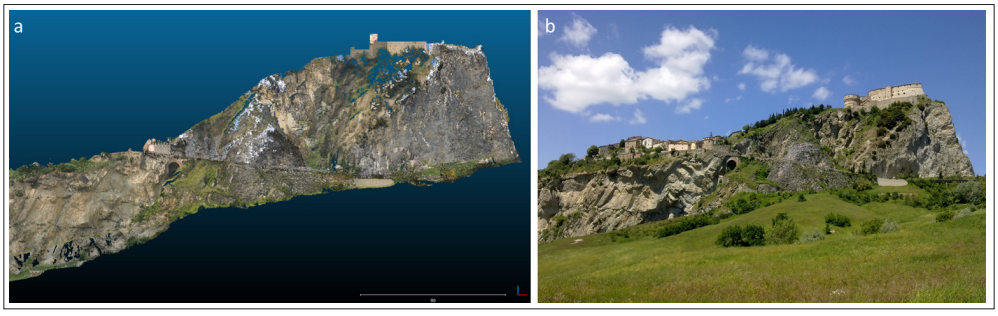

Figure 4 - a) TLS point cloud of the south cliff; b) view of the south cliff.

Close-Range Photogrammetry (CRP)

The photogrammetric survey was carried out in two selected areas, applying the Structure for Motion (SfM) technique. SfM, mainly developed in the Computer Vision community, operates under the same basic principles as stereoscopic photogrammetry: structure can be resolved from a series of overlapping, offset images. However, data acquisition differs from conventional photogrammetry as far as geometry of the scene, camera positions and orientation are concerned, together with the number of images acquired. Orientation parameters are solved simultaneously using a highly redundant iterative bundle adjustment procedure, based on automatic feature extraction from a set of multiple overlapping images [Westoby, 2012]. One of the key issues is related to the use of linear versus non-linear techniques to approach the geometric accuracy [Jebara et al., 1999].
The 3D models are generated, in the first step of SfM workflow, in a relative ‘image-

space' coordinate system, which must be aligned to a real world, 'object-space', coordinate system. As well as photogrammetry, the transformation of SfM image-space coordinates to an absolute coordinate system can be achieved using known Ground Control Points (GCPs) with known object-space coordinates. In this work, in order to optimize survey costs, the GCPs were derived from features clearly identifiable in the TLS point cloud. This method is less precise with respect to the use of a dedicated topographic survey (i.e., with targets), but the final absolute accuracy can be considered adequate considering the objectives of the study. Indeed one of the goals of this study is to test a relatively low-cost procedure beside the TLS in order to perform geostructural analyses.
The scheme adopted in the image acquisition, using nadiral and convergent images, is shown in Figure 5. For both areas a Nikon D300 with 24 mm calibrated prime lens was used. In the northern cliff, three camera positions were chosen with a 10 m interspace and a distance of about 60 meters from the cliff. In the southern area it was possible to place the camera less than 25 m far from the cliff and the distance between the positions was about 9.3 m. Following the approach detailed above, for each position five photo acquisitions were made, focused to infinity and with different angles between the line of sight of the camera and the perpendicular to the cliff (0°/-5°/-10°/+5°/+10°). According to SfM guidelines, the maximum redundancy (and overlap) of images and a good angle for point extraction can be reached. For the northern cliff, 16 photographs were taken with final GSD of about 6.3 cm and horizontal overlap about 70%. For the southern cliff, 33 photographs were taken with final GSD of about 6.2 cm and horizontal overlap about 70% across the site. Relative accuracy was estimated in 0.5 pixel for both sites.
The commercial software Agisoft Photoscan Pro [Agisoft, 2014] has been used. During the image workflow processing, a properly-distributed network of 10 GCPs (extracted from TLS point cloud) was used in the bundle adjustment in order to obtain georeferenced models.

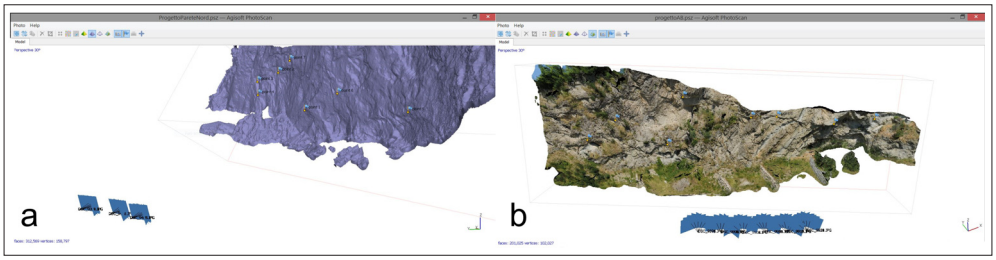

Figure 5 - Agisoft Photoscan software: a) Northern cliff: survey configuration with meshed model and GCPs; b) Southern cliff: camera positions, textured point cloud and GCPs.

The final root mean square total error referred to the point cloud georeferencing was about 0.27 m for the northern cliff and 0.40 m for the southern cliff. The northern cliff point cloud is composed by about 4.6 million points, while the southern cliff consists of about 3 million points. After model creation the consistence of the cliff model was checked by visual analysis. The models were exported as point clouds, and the georeferencing was refined applying the dedicated procedure in the CloudCompare [Girardeau-Montaut, 2014] software. Then the same procedure illustrated for the fracture mapping on TLS point clouds was adopted.

Discontinuity mapping

The structural characterization was performed directly on the 3D point clouds (both from TLS and CRP) using two different software, COLTOP 3D [Jaboyedoff et al., 2007] and Polyworks [Innovmetric, 2014]. The first displays the orientation of each vertex of the point cloud using an Intensity-Hue-Saturation coding in a stereographic projection; the result is a coloured shaded relief map combining both terrain slope angle and slope aspect (direction of slope) in a unique representation, which can assist in the characterization of potentially unstable slopes. In the Polyworks software, a manual method was used, fitting the recognized discontinuities with planes; the best-fit algorithm which performs a pure least-squares approach on all selected element points was used. This planar regression method is shown to be effective in calculating the orientation of planes from selected points of a point-cloud [De Souza et al., 2013]. Dip and dip direction were calculated from the equation planes coefficients.

Results and data comparison

The rock mass characterization was performed for each sector of the cliff. In the location where geomechanical, CRP and TLS surveys were performed (part of the northern and southern cliffs), a comparison between the outcomes of the different techniques is presented.

Conventional geomechanical survey

Results for the northern cliffs are shown in Table 1: three main joint sets plus several vertical discontinuities were identified. The Joint Roughness Coefficient (JRC) was deducted from the roughness profiles measured directly on discontinuities. The Schmidt hammer measurements permit to identify the Joint Compression Strength (JCS). Joint sets mean aperture and the presence of infilling are also reported. Similar results were produced for the southern area. In both cases the bedding was not identified.

Table 1 - Results of the conventional geomechanical survey carried on in the northern side of the slab. In the set name the first letter indicates the technique (Geomechanical survey), the second one the area (North).The set named TNV group all the identified vertical discontinuities.

ID Set SOUTH CLIFF	Dip [°]	Dip direction [°]	Variability angle (68%) [°]	Mean JRC	Mean JCS	Mean aperture [mm]	Infilling	Mean spacing [m]
GS1a	62	234	27	15	24.5	0.01	no	2.3
GS2	53	334	20	10	23.2	0.01	no	2.3
GS4	48	48	15	11	37.4	0.01	yes	1.4
ID Set NORTH CLIFF	**Dip [°]**	**Dip direction [°]**	**Variability angle (68%) [°]**	**Mean JRC**	**Mean JCS**	**Mean aperture [mm]**	**Infilling**	**Mean spacing [m]**
GN2	65	272	23	8.6	40.3	1.7	yes	0.5
GN3	75	25	19	9.0	38.3	0.01	no	1.9
GN4	67	67	16	10.0	39.7	0.6	yes	0.6
GNV	90	270	10	7	26.3	0.6	yes	1.25

TLS survey

Using the TLS point clouds, six main discontinuity sets were identified in the northern cliff, while five discontinuity sets were highlighted in the southern cliff. The bedding was detected in the two areas. Dip and dip direction of these sets are reported in Table 2.

Table 2 - Results of the discontinuity mapping on TLS point clouds. In the set name the first letter indicates the technique (terrestrial Laser scanner), the last one the area (North or South).

ID Set - SOUTH CLIFF	Dip [°]	Dip direction [°]	Variability angle (68%) [°]
LS1a	76	219	14
LS1b	64	256	12
LS2	65	298	17
LS3	74	179	16
LS4	56	43	15
LS6- bedding plane	25	25	16
ID Set - NORTH CLIFF	**Dip [°]**	**Dip direction [°]**	**Variability angle (68%)** [°]
LN1	62	240	17
LN2	72	293	9
LN3	83	10	12
LN4	63	42	20
LN5	64	95	17
LN6 - bedding plane	11	144	6
LN7	79	160	7

CRP survey

In the southern cliff, six sets plus the bedding planes were identified, while in the northern cliff six sets were grouped. The bedding planes were also measured. Results for the two areas are shown in Table 3.

Table 3 - Results of the discontinuity mapping on CRP point clouds. In the set name the first letter indicates the technique (Close-Range Photogrammetry), the last one the area (North or South).

ID Set – SOUTH CLIFF	Dip [°]	Dip direction [°]	Variability angle (68%) [°]
PS1a	82	214	12
PS1b	73	236	13
PS2	66	320	20
PS3	85	177	7°
PS4	55	31	18
PS6 - bedding plane	10	25	18
ID Set - NORTH CLIFF	**Dip [°]**	**Dip direction [°]**	**Variability angle (68%)**
PN1	67	227	14
PN2	73	295	6
PN3	84	11	13
PN4	59	38	21
PN5	65	104	20
PN6 - bedding plane	26	149	22
PN7	83	165	7

Comparison

The joint sets obtained from the three methods were compared (Fig. 6). Firstly, it is clear how certain features can be obtained only from a specific survey technique, e.g. the JCS can be measured only through geomechanical surveys, while the 3D model of the cliffs can be made available only using the remote sensing techniques.

Regarding the orientation of the discontinuities, some of the sets are recognized with all the techniques (sets 1a, 2 and 4 for the southern cliff; sets 2, 4, and 3 for the northern cliff, see Fig. 6), and not all of them were detected using the geomechanical survey alone.

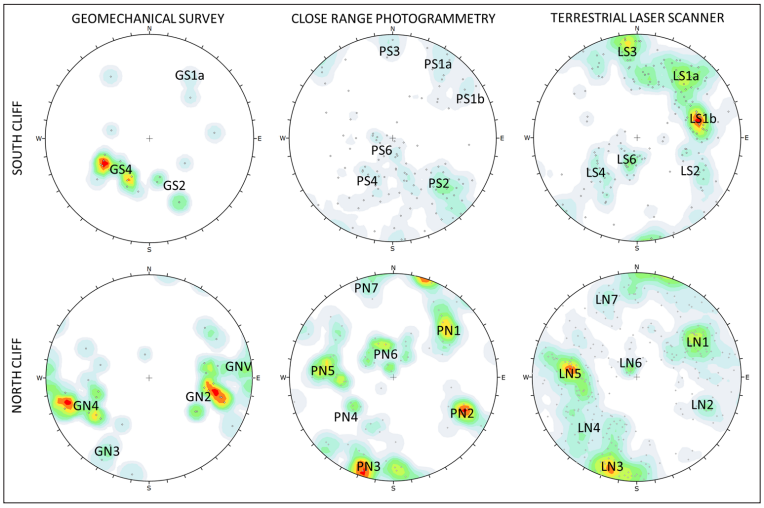

Figure 6 - Comparison between geomechanical survey, CRP and TLS in fracture mapping, for the south and north cliffs (equal angle stereonet).

This is probably due to the reduced extension of the area which can be investigated with geomechanical scanlines. As an example, the bedding plane was not identified by geomechanical surveys, probably because it is clearly visible only in inaccessible areas, at the top of the cliff. Instead, the conventional survey can be more effective in recognizing the fractures not clearly visible from the remote sensing surveys, e.g. when the fractures appear as traces and don't have an adequate relief [Sturzenegger and Stead, 2009a], or the visible plane is too small compared to the point spacing of the cloud or to the GSD. Results from the TLS and CRP are similar. A comparison between sections extracted from the two point clouds is presented in Figure 7. The TLS section (in red) is rougher, well describing the real asperity of the rock cliff, while the one from photogrammetry (in blue) is smoother, only approximating the real cliff face. The differences between surfaces can be due to many reasons, mainly related to the geometry of the acquisition scheme, to the presence of vegetation and to illumination factors in topographically complex surfaces, which are better captured by TLS systems. An alternative could be a UAV flight, which would permit horizontal acquisitions along the cliff [Tonkin et al., 2014; Genchi et al., 2015]. The final result is a less accurate surface compared to the one produced by the TLS: considering the whole point clouds of the southern cliff, an average distance of 0.03 m and a maximum distance of 1.40 m were measured using a nearest neighbor procedure in the CloudCompare software [Girardeau-Montaut, 2014].

Beside the above-mentioned issue of transforming the relative 3D model in one absolute system, model accuracy is also related to image texture and to a non-linear deformation which can limit the potential accuracy of SfM photogrammetry. Here, the aim is not to provide a full quantitative test of the accuracy and precision capabilities of the SfM, but to propose an application in the field of the geomechanical characterization of steep cliff faces. Indeed, it is still unclear how SfM-derived DEMs would perform in this field [Rango et al., 2009; Fonstad et al., 2013; Mancini et al., 2013]. More robust and quantitatively precise investigations under a wide range of geomorphic conditions will be necessary to establish the quality of SfM-derived DEMs for these purposes. Moreover, in the field of photogrammetry a number of further limitations are due to sunlight exposure over topographically complex surfaces (e.g., cavities, depressions, overhanging cliffs), which might be better tackled by laser scanning systems. Anyhow, the results are promising and show that the main issue is the smoothing effect on limited sectors of the point clouds (Fig. 7).

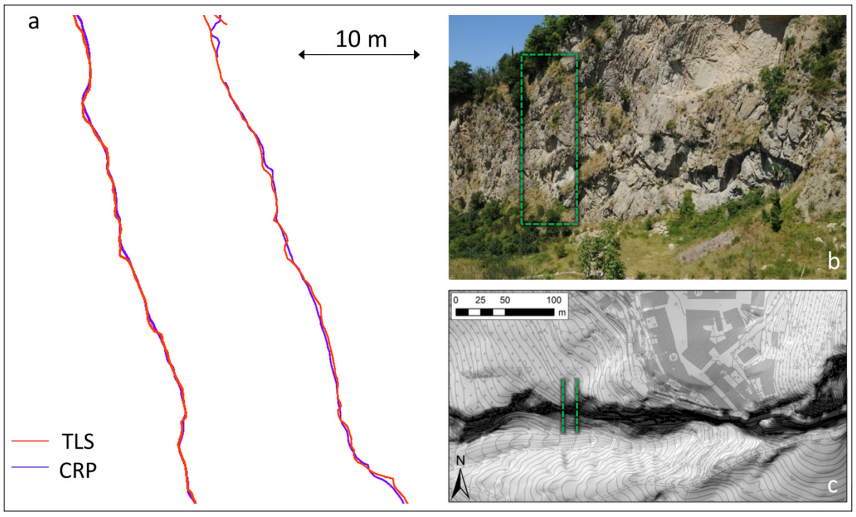

Figure 7 - a) Example of sections extracted from the CRP (purple) and TLS (red) point clouds; b, c) photoand DTM of the area with the sections localization.

Applications in the field of geological characterization

The 3D datasets obtained from the surveys were used in order to build a 3D model of the slab, to formulate hypotheses on its structural features at different scales and to perform a first assessment of slope stability. Hereafter two examples are presented: the first about the construction of a 3D model of the slab and the second in the field of slope stability analysis.

3D model of the slab

The TLS scans acquired on all the sides of the slab permit to reconstruct a full 3D model. The first alignment process was performed through the TLS software, Riscan Pro 2 [Riegl, 2014], using the target point coordinates obtained by the auxiliary survey and applying a rototraslation to the scans.

The root mean squares achieved during the alignment process are of the same order of magnitude of the GPS survey.

Due to the presence of a dense vegetation covering the cliffs, the Full Wave Form technology, implemented in the Riegl VZ-400 TLS, was adopted. This technology permits to discriminate and register different echo signals; point clouds can be then filtered, preserving only the single and last echos, which are more likely to match the real terrain. In this case study, the Full Wave Form technology was mostly effective in order to remove trees and bushes from the clouds, but for the grass and in general for small-scale vegetation covering the cliff, a heavy manual editing was still necessary.
The data were exported to Rapidform XOR3 [Inus Technology, 2012] software for the alignment refinement. The Iterative Closest Point (ICP) algorithm, which iteratively recomputes the transformation needed to minimize the distance between the points of two raw scans, was used. Then the scans of the 2013 surveys were joined with the ones from previous surveys, permitting to obtain a complete model of the cliffs.
Using this procedure, the 3D model of the San Leo slab was obtained. An attempt to assign an overall quality index to the whole model was made, although it was not straightforward, due to the complexity of the process and to the extension of the surveyed object. Regarding the accuracy achieved in the GNSS survey and in the alignment process, in the area surveyed between 2013 and 2014 (south and west cliffs) a maximum error around 2-3 centimeters can be considered. In the previous survey (north and east cliffs) the error could be higher, due to the instrumentation characteristics and the datum conversion needed to import the scans from the Gauss Boaga reference system into the UTM-WGS84 reference system. After cleaning and optimization procedures, the whole model is composed of 618,084,619 points. The obtained point cloud was subdivided in subsets, depending on the cliff orientation, to allow a more convenient use (Fig. 8). The 3D model of the cliff allows direct measurements to be made, to extract sections and prospects, making the rock slope analysis easier. Examples of sections are shown in Figure 7.

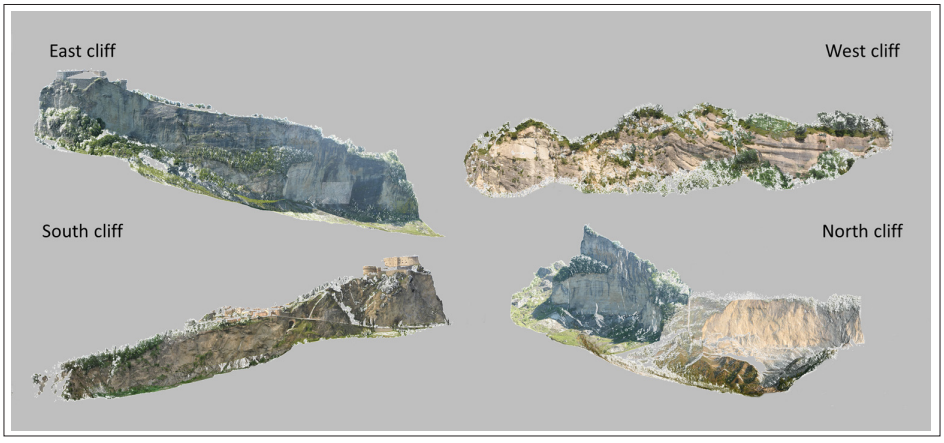

Figure 8 - Views of the TLS point cloud of the rock slab.

Structural characterization of the cliffs

The rock mass characterization was performed for each sector of the cliff. In Figure 9 a summary of the discontinuities mapped by means of TLS and CRP is reported. Surveys performed in the same cliff were grouped together, to offer a more general perspective. The

high number of discontinuities reported for the northern cliff is mostly due to the number of surveys conducted on this area (location of the last two main landslide events). Generally 5 or 6 joint sets plus the bedding plane were measured in all the areas, except for the more compact south-western sector. In particular, some areas were recognized as highly fractured with respect to the rest of the rock slab. These are closely related to the main structural lineaments recognized in the field. In particular, the south-eastern edge can be linked to the presence of a EW subvertical fault. Two highly fractured areas were recognized in the western side of the slab, in the southern and in the northern cliffs. They can be related to the NNW-SSE fault mapped in the field, also driving groundwater flow at the slab scale. As anticipated, the south-western part of the slab was instead recognized as less fractured: only scattered discontinuities and the bedding plane orientation were mapped. The different degree of fracturing between the northern and the southern area of the west cliff can suggest the presence of a WSW-ENE structural lineament.

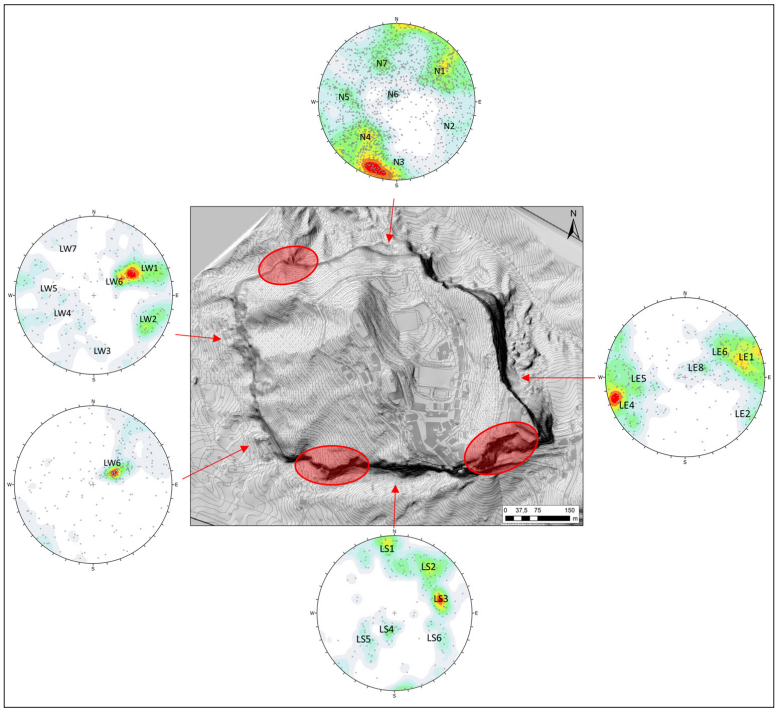

Figure 9 - Summary of the fracture mapping for each side of the slab. The high number of discontinuities reported for the North cliff is mostly due to the number of surveys conducted on this area (location of the last two main landslide events).The red circles represent the most fractured areas.

Some considerations can be drawn from the spatial distribution of the discontinuities. In the northern cliff most of the mapped discontinuities dip towards NNE or SSW. In the eastern cliff, fractures are mainly dipping ENE or WSW. In the southern cliff, fracture poles are mainly located in the NE sector of the stereographic projection. Thus, in almost all the sectors, a large percentage of discontinuities are dipping parallel to the cliff face. It

is worth to mention that, as discussed in Sturzenegger and Stead [2009a], some planes can be not clearly visible from the remote sensing surveys, e.g. when the fractures appear as traces (normal vector of the discontinuity plane parallel to the cliff face) and do not have an adequate relief. Therefore, the high percentage of discontinuities dipping parallel to the cliff faces can be due or to the characteristics of the adopted terrestrial remote sensing techniques or to the presence of subvertical discontinuities due to unloading and stress relief at the borders of the slab. For example, the sets LN3 and LS3, subvertical and parallel to the cliff orientation, can be interpreted as unloading joints. The presence of these features can assume a primary role in the developing of major slope instability events, e.g. the one occurred in 2014. In fact, Spreafico et al. [2015b] highlighted the importance of an almost vertical joint set, striking sub-parallel to the cliff orientation, in the onset of the 2014 failure. Furthermore, the same Authors showed how the collapse itself may lead to the development of tension cracks and to the aperture of joints with a similar orientation, predisposing the slope to further instability of the same type Spreafico et al. [2015b].

Kinematic analysis

The joint sets obtained by processing the TLS point clouds have been used together with the ones from geomechanical surveys to perform kinematic analyses. These were carried out using the Markland test procedure implemented in the Dips Software [Rocscience, 2014]. The method allows the kinematics driving the slope instability processes affecting the cliffs to be assessed among sliding, toppling and wedging. More in detail, results were able to evidence the joint sets influencing the instability in the 2006 landslide area, in the northern side of the slab. Several orientations can be recognized in each cliff, e.g. in the northern cliff slope dip direction varies from 15° to 330°. A classical analysis was conducted using an averaged value for the slope orientation (Fig. 10). Then, to account for this variation, the kinematic analyses were repeated maintaining a fixed dip angle (90°) and varying the slope dip direction between the actual range (Fig. 11). The percentage of discontinuity poles included in the critical area were reported as an indication of the probability of failure. The percentage was calculated separately for each joint set (number of critical joint in set N/ total number of joint in set N) and considering the amount of all the mapped discontinuities (total, represented in black). This permitted to highlight the most critical joint sets for each slope orientation. For the wedge sliding only the total results are reported.

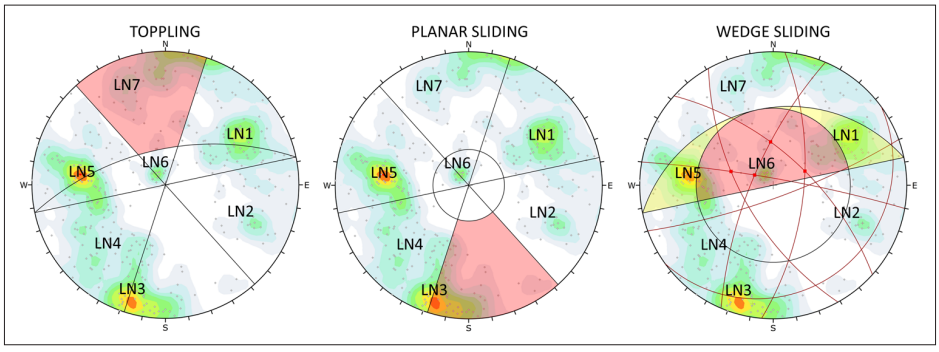

Figure 10 - Kinematic analysis (north cliff).

Discontinuities grouped in LN7 set could induce toppling phenomena as the poles cluster is included in the failure area. Set LN3 can both cause toppling or sliding. This dual behaviour depends on their almost vertical orientation; anyway, most of the discontinuities belonging to this subset are potential sliding surfaces.
Observing the point clouds, set LN5 and LN1 seem to behave as lateral release surfaces. Wedge sliding can occur due to the intersection of several subsets, namely LN1, LN2, LN3 (subvertical), LN4 and LN5. They allow the development of several wedges at the base of 2006 failure cliff, which are recognizable at different scales (Fig. 12). Examining the point cloud, it is clear that most of the existing wedges are formed by the intersection of two about 60° dip - subsets (LN5 and LN1) and the contemporary presence of the subvertical set LN3 and of a basal sliding surface. The two discontinuities do not intersect within the wedge sliding envelope in the kinematic analyses (Fig. 10), in fact the failure cannot be described through the classical wedge sliding definition, e.g. sliding along the intersection line of the two planes or on one of these. In this situation the sliding surface is represented by a failure plane developing within the underlying scaly clays, while the joints defining the wedge act as release surfaces.

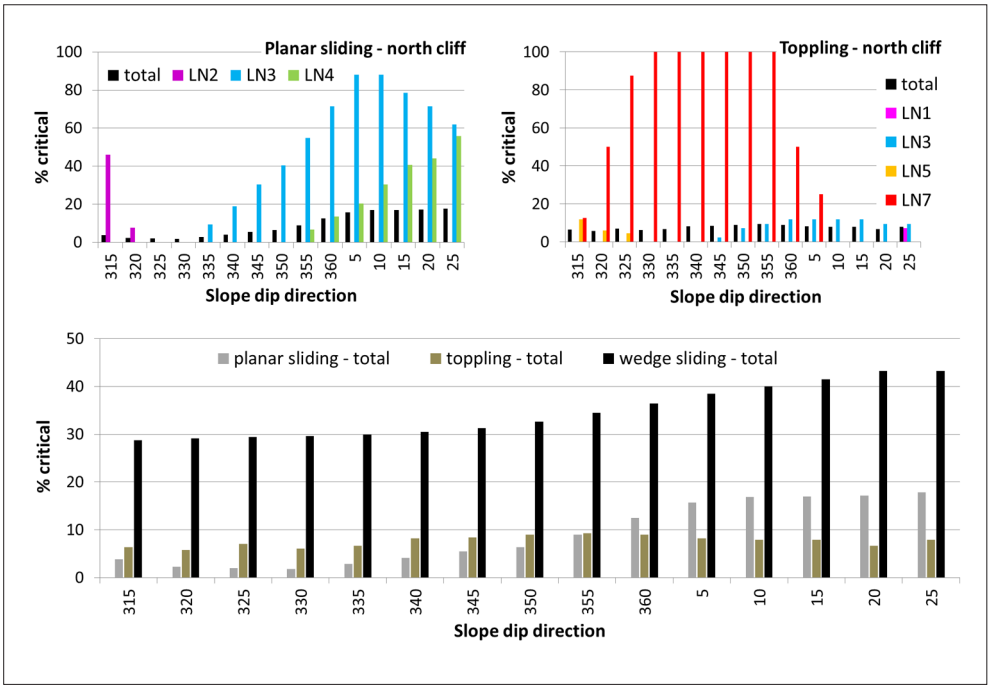

Figure 11 - Representation of the percentage of discontinuity poles included in the critical area for different slope dip directions (slope dip was fixed to 90°). The percentage was calculated separately for each joint set (number of critical joint in set N/total number of joint in set N) and considering the amount of all the mapped discontinuities (total).

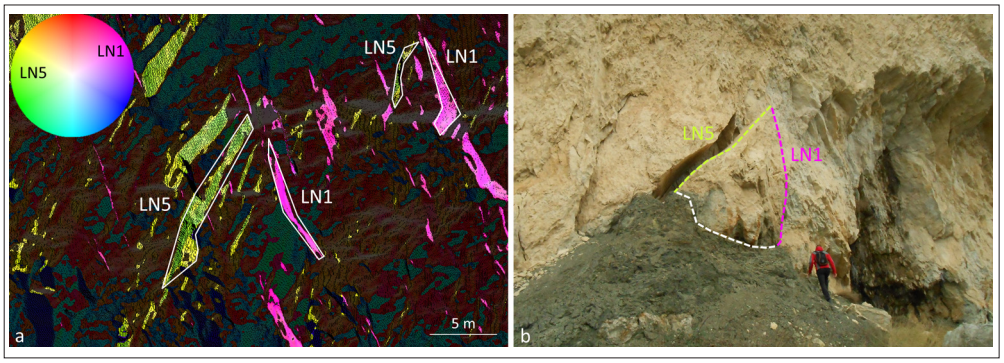

Figure 12 - Examples of wedges: a) recognized in the point cloud using the Coltop software and b) in the field.

Discussion

The results highlight the importance of the integration of different survey techniques to obtain a full representation of the 3D geometry of a geological object and a characterization of its discontinuities. The comparison of the results allows the main strength and limitations of each procedure to be confirmed. The TLS and CRP surveys permitted to obtain, at different scales, the 3D geometry of the cliff, which is not possible to determine with the conventional methods.

As discussed beforehand, due to the limited extension of the accessible areas, data from conventional surveys are often scarce. This limitation can assume a particular importance in case of irregularly jointed rock masses, where discontinuities measured in a small areas cannot be representative of the whole rock mass [Sturzenegger and Stead, 2009a]. Comparing these surveys with the most extensive TLS and CRP data, some discontinuities characteristics, e.g. the aperture, can be inferred also in areas where direct measures are not feasible.

Concerning the remote sensing techniques, although TLS is to be considered more accurate, CRP provided adequate data regarding the rock mass. The results are in agreement with previous works by other Authors [Ravanel and Curtaz, 2013; Assali et al., 2014].

Regarding the feasibility of the surveys, the flexibility and the handiness of the CRP with respect to a TLS survey is to be highlighted: even if the equipment used for the control points survey is the same in both cases, transporting the TLS system on an impervious terrain can be more difficult with respect to a digital camera.

The two methods should be used at different scales, allowing fractures with different persistence to be recognized. Based on the results, Figure 13 shows an indication of the scale at which the use of the different techniques is considered to be convenient; both technical and economic issues are qualitatively considered. The conventional survey techniques are more applicable at the outcrop scale. As indicated also by Sturzenegger and Stead [2009a], dealing with smaller areas, more measures can be provided from the conventional methods, whereas data acquired along virtual scanlines are limited by the resolution of the point cloud.

In order to be effective, remote sensing techniques have to cover a larger portion of the cliff. CRP is indicated for large outcrops or at the cliff scale, due to the flexibility of the acquisition and to the obtained precision, almost comparable with the TLS one in the

field of the geological discontinuities characterization. When dealing with a large cliff or with an entire rock slab, the TLS technique is to be preferred, allowing a large number of measurements in a relative smaller amount of time to be collected, maintaining a sufficient precision also from long distances (about some hundreds of metres). The coupling with Unmanned Aerial Vehicle (UAV) could eventually extend the use of CRP, thus covering a wider range of scales. If the scale analysis decrease, typical geomorphological point of view could be covered by using other geomatics techniques such as ALS and/or Aerial Photogrammetry [Lucchesi et al., 2013; Bacenetti et al., 2015].

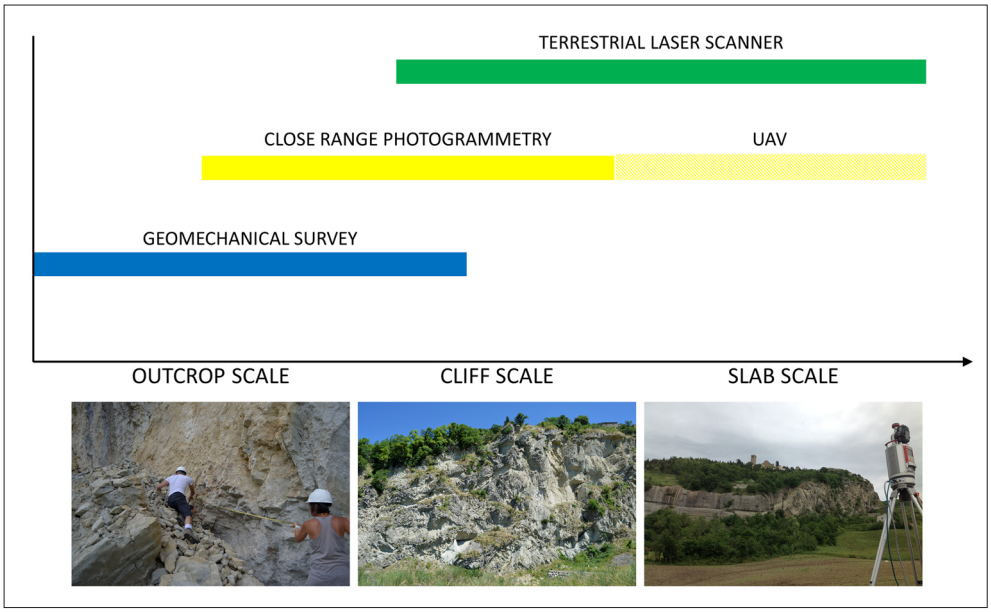

Figure 13 - Use of the three techniques at different scales.

These general indications can help in the choice of the convenient method, but each different case has to be carefully evaluated, considering all the variables which can influence the final decision. Among them, the topography and the accessibility of the area, the purpose of the survey and the characteristics required for the final products should be taken into account for the survey planning. Finally, a further advantage of the remote sensing techniques consisted in the possibility to observe and analyse the point clouds whenever measurements or comparisons with other datasets were needed. Previous acquisitions can in fact be compared with new scans, making the monitoring of the cliff possible, along with the estimation of the volume of newly-formed landslides.

The use of stereographic techniques is only the first step in the characterization of the cliff. In fact, the dataset acquired using conventional and remote sensing surveys provides a good description of the joint properties, which can be used to carry out more complex analyses. The structural data from the TLS point cloud have been used to define different structural domains within the plateau and for kinematic analysis in the area of the 2006 landslide.

The definition of the main lineaments is also useful to improve the hydrogeological model of

the plateau. In fact, fault areas usually have a different hydraulic conductivity with respect to the surrounding rock mass and depending from the presence and type of infilling they could behave as permeable or impermeable barriers. The information about the discontinuities aperture, gained from the traditional survey and extended to the whole rock mass thanks to the TLS dataset, can be used to estimate an initial value for the equivalent permeability. In fact, these data were used, together with the geometry of the slab and the mean discontinuities orientation, as input for a 3D hydrogeological model [Spreafico et al., 2015a].
In order to build up a more complex slope stability model, the strength properties of the discontinuities are required. These can be estimated using the joints roughness and compression strength. The first can be estimated both in the field and extracting discontinuities profiles from remote sensing point clouds, although it can be difficult to estimate the small-scale roughness [Wolter et al., 2013]. The JCS can be easily obtained during traditional survey for each discontinuity, and then the averaged value can be associated to the specific joint set. Furthermore, the 3D point clouds derived from the TLS survey were used to build a 3D model of the slab. In fact, Francioni et al. [2014] highlight the advantages of using geometrical models obtained from terrestrial remote sensing instead of the ones based on topographic maps, in the framework of slope stability modelling. This applies particularly in case of vertical and overhanging cliffs, where the factor of safety computed on the geometry extracted from topographic maps can be overestimated up to the 10%.

Conclusions

With the aim to preserve the notable natural and cultural heritage of San Leo village, understanding slope processes and their evolution is of fundamental importance. One of the main predisposing factors of slope instability phenomena affecting the rock slab is certainly its geological and structural setting, which is characterized by several discontinuities, namely bedding planes, joints and faults. Usually, geomechanical surveys are performed along scanlines or through observation windows, directly on the outcrops. In extreme geological contexts (i.e., large and unstable rocky cliffs), only a limited number of measurements can be collected with these conventional methods. In fact, the surveys are often concentrated in small areas, which may be not representative of the entire rock mass. Moreover, certain sets may change their orientation along the slope surface. For these reasons, the integration of conventional and innovative surveying techniques can be really useful to obtain a complete picture. In San Leo rocky plateau, dense Digital Surface Models (DSMs) obtained from CRP and TLS surveys, complemented with geomechanical surveys, were used to understand which sets are determinant for the description of the structural features at the slope scale and for the assessment of slope instability mechanisms in critical areas. The creation of a 3D model was also fundamental for the implementation of the geological model to be used in numerical modelling for hydrogeological and slope stability analyses.

Acknowledgments

The Authors wish to thank Dr. Claudio Corrado Lucente (Servizio Tecnico Bacino di Romagna, the technical board of Emilia-Romagna Region), for making the TLS surveys 2008-2011 available to complete the 3D model of the area. Suggestions by Prof. Monica Ghirotti on rock mass characterization were appreciated.

References

Abellán A., Vilaplana J. M., Martínez J. (2006) - *Application of a long-range Terrestrial Laser Scanner to a detailed rockfall study at Vall de Núria (Eastern Pyrenees, Spain)*. Engineering Geology, 88 (3-4): 136-148. doi: http://dx.doi.org/10.1016/j.enggeo.2006.09.012.

Agisoft LLC (2014) - *Agisoft Photoscan Pro*. St. Petersburg, Russia. Available online at: http://www.agisoft.com.

Assali P., Grussenmeyer P., Villemin T., Pollet N., Viguier F. (2014) - *Surveying and modeling of rock discontinuities by terrestrial laser scanning and photogrammetry: Semi-automatic approaches for linear outcrop inspection*. Journal of Structural Geology, 66: 102-114. doi: http://dx.doi.org/10.1016/j.jsg.2014.05.014.

Bacenetti M., Spreafico M., Elettri F., Giardino M., Perotti L., Borgatti L., Ghirotti M., Ratto S. (2015) - *Geomorphological Analyses, Geomatic Surveys and Numerical Modelling for the Characterization of the Chervaz Deep-Seated Gravitational Slope Deformation, Chambave (AO)*. In: Lollino G., Giordan D., Crosta G.B., Corominas J., Azzam R., Wasowski J., Sciarra N. (Eds.), Engineering Geology for Society and Territory, 2 (VII): 565-569. doi: http://dx.doi.org/10.1007/978-3-319-09057-3_93.

Barbarella M., Fiani M. (2013) - *Monitoring of large landslides by terrestrial laser scanning techniques: field data collection and processing*. European Journal of Remote Sensing, 46: 126-151. doi: http://dx.doi.org/10.5721/EuJRS20134608.

Barton N.R., Choubey V. (1977) - *The shear strength of rock joints in theory and practice*. Rock Mech., 10 (1-2): 1-54. doi: http://dx.doi.org/10.1007/BF01261801.

Benedetti G., Bernardi M., Bonaga G., Borgatti L., Continelli F., Ghirotti M., Guerra C., Landuzzi A., Lucente C.C., Marchi G. (2013) - *San Leo: centuries of coexistence with landslides*. Landslide Science and Practice, 6: 529-528. doi: http://dx.doi.org/10.1007/978-3-642-31319-6.

Bistacchi A., Griffith W. A., Smith S.A.F., Di Toro G., Jones R., Nielsen S. (2011) - *Fault Roughness at Seismogenic Depths from LIDAR and Photogrammetric Analysis*. Pure and Applied Geophysics, 168 (12): 2345-2363. doi: http://dx.doi.org/10.1007/s00024-011-0301-7.

Bitelli G., Dubbini M., Zanutta A. (2004) - *Terrestrial laser scanning and digital photogrammetry techniques to monitor landslide bodies*. International Archives of the Photogrammetry, Remote Sensing and Spatial Information Sciences, XXXV-B: 246-251.

Borgatti L., Guerra C., Nesci O., Romeo R.W., Veneri F., Benedetti G., Landuzzi A., Marchi G., Lucente C.C. (2015) - *The 27 February 2014 San Leo rock fall (northern Italy)*. Landslides, 12 (2): 387-394. doi: http://dx.doi.org/10.1007/s10346-015-0559-4.

Bozzano F., Bretschneider A., Martino S. (2008) - *Stress-strain history from the geological evolution of the Orvieto and Radicofani cliff slopes (Italy)*. Landslides, 5 (4): 351-366. doi: http://dx.doi.org/10.1007/s10346-008-0127-2.

Casagli N. (1994) - *Fenomeni di instabilità in ammassi rocciosi sovrastanti un substrato deformabile: analisi di alcuni esempi nell'Appennino settentrionale*. II Convegno Nazionale dei Giovani ricercatori di Geologia Applicata, Viterbo.

Coggan J.S., Wetherelt A., Gwynn X.P., Flynn Z. (2007) - *Comparison of hand-mapping with remote data capture systems for effective rock mass characterisation*. Proceedings of 11th Congress of the International Society for Rock Mechanics - The Second Half

Century of Rock Mechanics, 1: 201-205.

De Souza M.K., Veronez F.M., Tognoli W., Da Silveira Jr.L.G., Inociencio L.C., Da Silva R.M., Modena R.C.C. (2013) - *Terrestrial Laser Scanning: Application for Measuring of Structures Information in Geological Outcrops*. International Journal of Advanced Remote Sensing and GIS, 2 (1): 260-270.

Di Salvo F., Lo Brutto M. (2014) - *Full-Waveform Terrestrial Laser Scanning for Extracting a High-Resolution 3D Topographic Model: a Case Study on an Area of Archaeological Significance*. European Journal of Remote Sensing, 47: 307-327. doi: http://dx.doi.org/10.5721/EuJRS20144719.

Ferrero A.M., Forlani G., Rondella R., Voyat H.I. (2009) - *Advanced geostructural survey methods applied to rockmass characterization*. Rock Mechanics and Rock Engineering, 42: 631-665. doi: http://dx.doi.org/10.1007/s00603-008-0010-4.

Fonstad M.A., Dietrich J.T., Courville B.C., Jensen J.L, Carbonneau P.E. (2013) - *Topographic structure from motion: A new development in photogrammetric measurement*. Earth Surface Processes and Landforms, 38 (4): 421-430. doi: http://dx.doi.org/10.1002/esp.3366.

Genchi S.A., Vitale A.J., Perillo G.M., Delrieux C.A. (2015) - S*tructure-from-motion approach for characterization of bioerosion patterns using UAV imagery*. Sensors, 15 (2): 3593-3609. doi: http://dx.doi.org/10.3390/s150203593.

Giardino M., Perotti L., Bacenetti M., Zamparutti P. (2011) - *Climatic and structural controls to slope instabilities in the Veny valley (Mont Blanc): new insights by integrating field-based, Lidar and Remote Sensing techniques*. The Second World Landslide Forum - Abstract Book, ISPRA, Roma, pp. 661- 661.

Girardeau-Montaut D. (2014) - *CloudCompare.* Available on line at: http://www.danielgm.net/cc/.

Humair F., Pedrazzini A., Epard J.L., Froese C.R., Jaboyedoff M. (2013) - *Structural characterization of Turtle Mountain anticline (Alberta, Canada) and impact on rock slope failure*. Tectonophysics, 605: 133-148. doi: http://dx.doi.org/10.1016/j.tecto.2013.04.029.

InnovMetric Software (2014) - *Polyworks version 2014*. Quebec City, Canada. Available on line at: http://www.innovmetric.com/.

Inus technology (2012) - *Rapidform XOR3*. Seoul, South Corea. Available on line at: http://www.rapidform.com/home/.

ISRM Commission on Testing Methods (1978) - S*uggested methods for the quantitative description of discontinuities in rock masses*. International Journal of rock Mechanics and Mining Sciences and Geomechanics Abstracts, 15 (6): 319-368.

Jaboyedoff M., Metzger R., Oppikofer T., Couture R., Derron M.-H., Locat J.,Turmel D. (2007) - *New insight techniques to analyze rock-slope relief using DEM and 3D-imaging cloud points: COLTOP-3D software*. In: Eberhardt E., Stead D., Morrison T. (Eds.), Rock mechanics: Meeting Society's Challenges and demands, 1: 61-68. doi: http://dx.doi.org/10.1201/NOE0415444019-c8.

Jaboyedoff M., Oppikofer T., Abellán A., Derron M.H., Loye A., Metzger R., Pedrazzini A. (2010) - *Use of LIDAR in landslide investigations: a review*. Natural Hazards, 61: 5-28. doi: http://dx.doi.org/10.1007/s11069-010-9634-2.

Jebara T., Azarbayjani A., Pentland A. (1999) - *3D Structure from 2D Motion*. IEEE Signal Processing Magazine,"3D And Stereoscopic Visual Communication", 16 (3).

Lucchesi S., Giardino M., Perotti L. (2013) - *Applications of high-resolution images and DTMs for detailed geomorphological analysis of mountain and plain areas of NW Italy*. European Journal of Remote Sensing, 46: 216-233. doi: http://dx.doi.org/10.5721/EuJRS20134612.

Mancini F., Dubbini M., Gattelli M., Stecchi F., Fabbri S., Gabbianelli G. (2013) - *Using Unmanned Aerial Vehicles (UAV) for High-Resolution Reconstruction of Topography: The Structure from Motion Approach on Coastal Environments*. Remote Sensing, 5 (12): 6880-6898. doi: http://dx.doi.org/10.3390/rs5126880.

Matasci B., Ravanel L., Jaboyedoff M., Deline P. (2012) - *Structural analysis and stability assessment of the West face of the Drus (3733m, Mont Blanc massif)*. Geophysical Research Abstracts, 14 (EGU2012-12331-1).

Nex F., Rinaudo F. (2011) - *LiDAR or Photogrammetry? Integration is the answer*. Italian Journal of Remote Sensing, 43: 107-121. doi: http://dx.doi.org/10.5721/ItJRS20114328.

Nguyen H., Fernandez-Steeger T., Wiatr T., Rodrigues D., Azzam R. (2011) - *Use of terrestrial laser scanning for engineering geological applications on volcanic rock slopes - an example from Madeira island (Portugal)*. Natural Hazards and Earth System Science, 11: 807-817. doi: http://dx.doi.org/10.5194/nhess-11-807-2011.

Oppikofer T., Jaboyedoff L., Blikra R., Derron M., Metzger R. (2009) - *Characterization and monitoring of the Aknes rockslide using terrestrial laser scanning*. Natural Hazard and Earth System Science, 9: 1003-1019. doi: http://dx.doi.org/10.5194/nhess-9-1003-2009.

Pasuto A., Soldati M. (2013) - *Lateral Spreading*. Treatise on Geomorphology, 7: 239-248. doi: http://dx.doi.org/10.1016/B978-0-12-374739-6.00173-1.

Rango A., Laliberte A., Herrick J.E., Winters C., Havstad K., Steele C., Browning D. (2009) - *Unmanned aerial vehicle-based remote sensing for rangeland assessment, monitoring, and management*. Journal of Applied Remore Sensing, 3 (1): 033542. doi: http://dx.doi.org/10.1117/1.3216822.

Ravanel L., Curtaz M. (2013) - *Action 6.1 - Comparison of methods Terrestrial Laser scanning/Terrestrial Photogrammetry*. Permafrost long term monitoring network project. Available on line at: http://www.permanet-alpinespace.eu/.

Riegl (2014) - *Riscan pro 2*. Horn, Austria. Available on line at: http://www.riegl.com/nc/.

Rocscience (2014) - *Dips version 6.0*. Rocscience Incorporation, Toronto, Canada. Available on line at: https://www.rocscience.com.

Spreafico M.C., Girelli V.A., Lucente C.C., Tini M.A., Bitelli G., Borgatti L. (2014) - *Terrestrial Laser Scanner data for landslide hazard assessment in the cliff of San Leo (northern Apennines, Italy).* Geology and Information Technology 16-18/6/14 Montefalco, PG, Italy.

Spreafico M.C., Cervi F., Petronici F., Borgatti L. (2015a) - *Modelling groundwater and slope processes in a calcarenitic slab: the case of San Leo (northern Apennines)*. Rendiconti Online della Società Geologica Italiana, 34: 283-287. doi: http://dx.doi.org/10.33.01/ROL.2015.31.

Spreafico M.C., Francioni M., Cervi F., Stead D., Bitelli G., Ghirotti M., Girelli V.A., Lucente C.C., Tini M.A., Borgatti L. (2015b) - *Back Analysis of the 2014 San Leo Landslide Using Combined Terrestrial Laser Scanning and 3D Distinct Element Modelling*. Rock Mechanics and Rock Engineering, 763. doi: http://dx.doi.org/10.1007/

s00603-015-0763-5.

Sturzenegger M., Stead D. (2009a) - *Close-range terrestrial digital photogrammetry and terrestrial laser scanning for discontinuity characterization on rock cuts*. Engineering Geology, 106 (1): 163-182. doi: http://dx.doi.org/10.1016/j.enggeo.2009.03.004.

Sturzenegger M., Stead D. (2009b) - *Quantifying discontinuity orientation and persistence on high mountain rock slopes and large landslides using terrestrial remote sensing techniques*. Special Issue: Natural Hazards and Earth Systems Science, 9: 267-287. doi: http://dx.doi.org/10.5194/nhess-9-267-2009.

Tonkin T.N., Midgley N.G., Graham D.J., Labadz J.C. (2014) - *The potential of small unmanned aircraft systems and structure-from-motion for topographic surveys: a test of emerging integrated approaches at Cwm Idwal, North Wales*. Geomorphology, 226: 35-43. doi: http://dx.doi.org/10.1016/j.geomorph.2014.07.021.

Wolter A., Stead D., Clague J.J. (2013) - *A morphologic characterisation of the 1963 Vajont Slide, Italy, using long-range terrestrial photogrammetry*. Geomorphology, 206: 147-164. doi: http://dx.doi.org/10.1016/j.geomorph.2013.10.006.

Westoby M.J., Brasington J., Glasser N.F., Hambrey M.J., Reynolds J.M. (2012) - *'Structure-from-Motion' photogrammetry: A low-cost, effective tool for geoscience applications*. Geomorphology, 179: 300-314. doi: http://dx.doi.org/10.1016/j.geomorph.2012.08.021.

Zhang L., Einstein H.H. (1998) - *Estimating the Mean Trace Length of Rock Discontinuities*. Rock Mechanics and Rock Engineering, 31, 4: 217-235. doi: 10.1007/s006030050022.

Zhang L., Einstein H.H. (2000) - *Estimating the intensity of rock discontinuities*. International Journal of Rock Mechanics and Mining Sciences, 37, 5: 819-837. doi: http://dx.doi.org/10.1016/S1365-1609(00)00022-8.